$e^+e^- \to \tau^+\tau^-$ production and the $\tau \to e\nu\nu$ BR measurement at Belle II

Yin Tan, Chongqing University, China

Supervisor: Petar Rados

September 4, 2019

Abstract

This report describes the reconstruction of τ-pair production events and the measurement of the $\tau \to e\nu\nu$ branching ratio at Belle II .[1] The e^+e^- collision data used in this study was recorded during Phase III and corresponds to 1.9 fb^{-1}. After the trigger and offline selections, the branching ratio of $\tau \to e\nu\nu$ has been determined to be $(17.46 \pm 0.16)\%$, in reasonable agreement with the PDG value.

Contents

1 Introduction

The tau lepton is an elementary particle similar to the electron, with negative electric charge and a spin of 1/2. It has a corresponding antiparticle of opposite charge but equal mass and spin, which is called antitau (also called the positive tau). Tau leptons are denoted by τ^- and the antitau by τ^+. At Belle II, the cross section of the process $e^+e^- \to \tau^+\tau^-$ at the $\Upsilon(4S)$ resonance energy is of the same order as the production of a B pair from the e^+e^- collision. In this way, Belle II is not only a B-factory but also a τ lepton factory.

The τ lepton has a mass of 1776.86 MeV which is far greater than the muon and electron (compared to 105.66 MeV for the muon and 0.511 MeV for the electron), and so the τ is the only lepton that can decay into hadrons. The τ lepton has a lifetime of 2.9×10^{-13} s, due to their short lifetime, tau leptons will decay before reaching the active regions of the Belle II detector and so are reconstructed via their decay products. Tau leptons mainly decay into charged pions, muons or electrons in association with neutrinos.

The analysis targets $e^+e^- \to \tau^+\tau^-$ events, where one tau lepton decays leptonically with an electron ($\tau^- \to e^-\bar{\nu}_\tau\nu_e$) while the other decays hadronically into three charged pions ($\tau^+ \to \pi^+\pi^-\pi^+\nu_\tau + n\pi^0$). These decays will be referred to, hereafter, as the 1-prong and 3-prong decays, respectively. The Feyman diagram for the targeted process is shown in Figure 1.

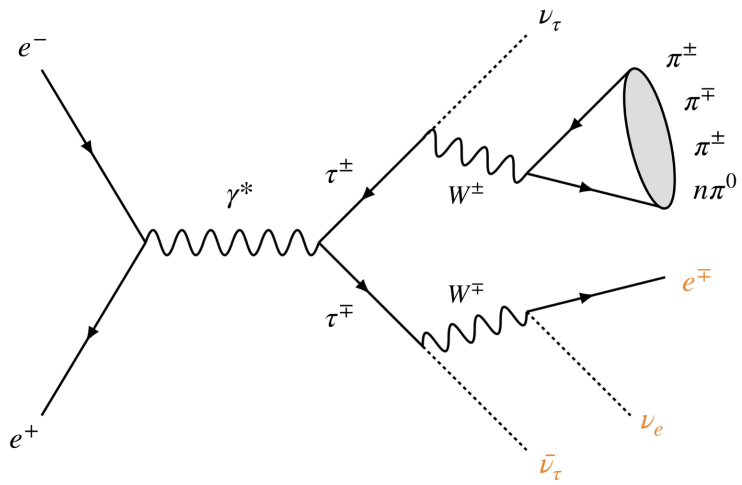

Figure 1: Feyman diagram of $e^+e^- \to \tau^+\tau^-$ events. The 1-prong decay is highlighted in orange.

This report presents preliminary results on the reconstruction of τ-pair events, and the $\tau^- \to e^-\bar{\nu}_\tau\nu_e$ branching ratio measurement using Phase III reprocessed e^+e^- collision data from Belle II.

2 Accelerator and Detector

The Belle II experiment [2] is an upgrade of the Belle detector that is coupled to the SuperKEKB collider located in Tsukuba, Japan. SuperKEKB is an energy asymmetric electron-position collider operating at $\sqrt{s} = 10.58$GeV that corresponds to the $\Upsilon(4S)$ resonance energy. The accelerator can reach a 50nm vertical beam spot size during collisions, allowing it to reach an unprecedented instantaneous luminosity of $8.0 \times 10^{35} cm^{-2} s^{-1}$, which is 40 times higher then KEKB. A schematic diagram of SuperKEKB is shown in Figure2.

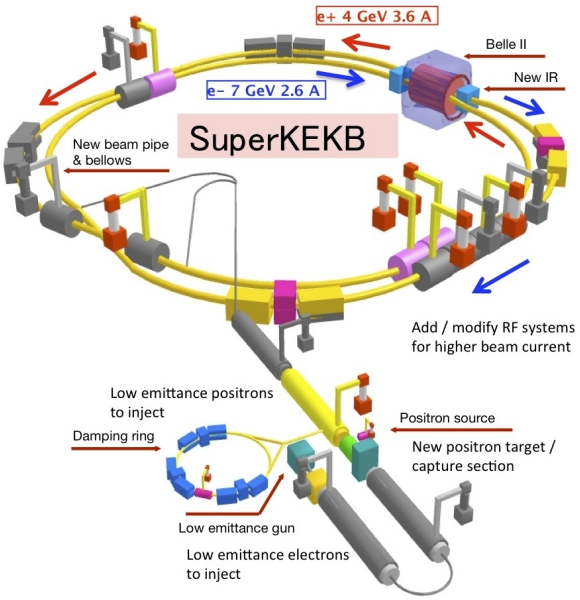

Figure 2: SuperKEKB accelerator

Belle II [3] consists of various detector components designated for specific purpouses (see Figure 3). The pixel detector (PXD) and silicon vertex detector (SVD) enable the tracking and vertexing of charged particles. The central drift chamber (CDC) can measure the trajectories, momenta and dE/dx of charged particles. Particle identification is perfomred by the time of propagation (TOP) counters and ring-imaging Cherenkov counters (A-RICH). Energy deposits are measured by the electromagnetic calorimeter (ECL) and K_L^0 mesons and muons are identified by the KLM.

3 Data and MC samples

This analysis was performed on e^+e^- collision data recored by Belle II during the Phase III period of data taking. More specifically, the proc9 data from Experiment 8 was used, corresponding to an integrated luminosity of $1982.3 \pm 0.6\ pb^{-1}$. The analysis

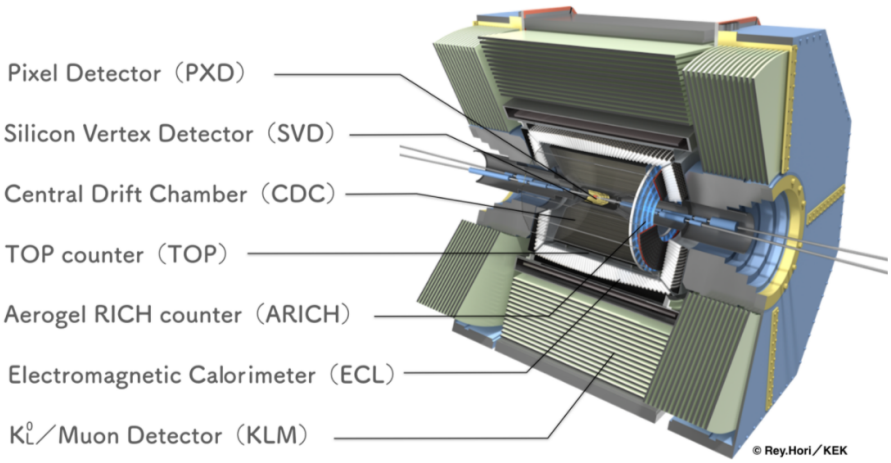

Figure 3: Belle II detector, highlighting the main sub components.

was performed using release-03-01-00 of the Belle II analysis software framework ($basf2$) with global tag $data\_reprocessing\_proc9$.

The official Phase III MC12 productions (see Table1) with the background condition BGx1 (nominal beam background conditions) were used for the event selection and background suppression studies. Details of the MC12 samples are described at https://confluence.desy.de/display/BI/Data+Production+MC12

Sample	$\int Ldt$	/belle/MC/release-03-01-00/DB00000547/MC12b/
taupair	80 fb^{-1}	prod00007809/s00/e1003/4S/r00000/taupair/mdst/sub00
uubar	80 fb^{-1}	prod00007801/s00/e1003/4S/r00000/uubar/mdst/sub00
ddbar	80 fb^{-1}	prod00007803/s00/e1003/4S/r00000/ddbar/mdst/sub00
ssbar	80 fb^{-1}	prod00007805/s00/e1003/4S/r00000/ssbar/mdst/sub00
ccbar	80 fb^{-1}	prod00007807/s00/e1003/4S/r00000/ccbar/mdst/sub00
ee	0.167 fb^{-1}	prod00007464/s00/e1003/4S/r00000/3900520000/mdst/sub00
eeee	5.30 fb^{-1}	prod00007464/s00/e1003/4S/r00000/3900520000/mdst/sub00
eemumu	5.29 fb^{-1}	prod00007465/s00/e1003/4S/r00000/3900420000/mdst/sub00
mumu	47.9 fb^{-1}	prod00007466/s00/e1003/4S/r00000/3500420000/mdst/sub00
pipi	1139.4 fb^{-1}	prod00007469/s00/e1003/4S/r00000/3700001000/mdst/sub00

Table 1: Phsae III MC12 samples used in the analysis

4 Selections

4.1 Candidate event pre-selections

In the $e^+e^- \to \tau^+\tau^-$ centre-of-mass system (CMS), both τ leptons are boosted and their decay products are well separated in two opposite hemispheres defined by the plane perpendicular to the thrust axis. The thrust axis n_{thrust} is defined such that the value V_{thrust}

$$V_{thrust} = \sum_i \frac{|\vec{p_i} \cdot \hat{n}_{thrust}|}{\sum \vec{p_i}}, \tag{1}$$

is maximized. Here, $\vec{p_i}$ is the CMS momentum of each charged particle and photon. Given the vector $\hat{n}_{thrust}$ that splits the event into two hemispheres, the signal hemisphere is expected to contain the 1-prong decay (see orange side of Figure4), while the tag side is expected to contain the 3-prong decay (see blue side of Figure4).

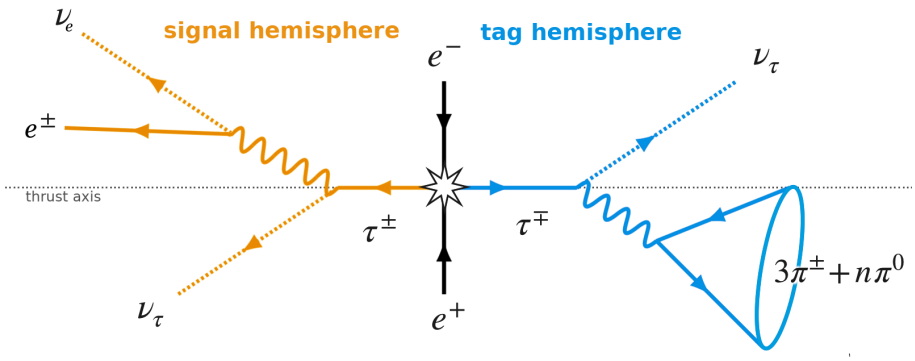

Figure 4: Feyman diagram on 1-prong side and 3-prong side

The candidate events are selected by requiring only four charged tracks in the event with zero net charge. Each track should satisfy the following requirements:

- The magnitude of the longitudinal impact parameter is required to satisfy $|dz| < 5$ cm
- The transverse impact parameter is required to satisfy $dr < 2.0$ cm

Since electrons will deposit almost all of their energy in the ECL, the signal side track is required to satisfy $E/P > 0.8$, where E is the energy deposit in the ECL and P is the momentum of the particle in laboratory system. The tag side tracks originate from pions, and so they are required to satisfy $0 < E/P < 0.8$.

Photon pairs with energy down to 100 MeV that satisfy $115 < M_{\gamma\gamma} < 152$ MeV are reconstructed as π^0. We also accept any additional photons with energy above 200 MeV.

4.2 Background suppression

There are processes other than τ-pair production that can satisfy the selection criteria discribed earlier. The list of background processes that can contaminate the τ-pair production sample are listed in Table2. We apply additional selections with the goal of suppressing these backgrounds.

Processes	Cross section[nb]	Name of the production
$e^+e^- \to u\bar{u}$	1.61	'uubar'
$e^+e^- \to d\bar{d}$	0.4	'ddbar'
$e^+e^- \to s\bar{s}$	0.38	'ssbar'
$e^+e^- \to c\bar{c}$	1.3	'ccbar'
$e^+e^- \to e^+e^-\gamma$	300 ± 3	'ee'
$e^+e^- \to \mu^+\mu^-\gamma$	1.148	'mumu'
$e^+e^- \to e^+e^-e^+e^-$	39.7 ± 0.1	'eeee'
$e^+e^- \to e^+e^-\mu^+\mu^-$	18.9 ± 0.1	'eemumu'
$e^+e^- \to \pi^+\pi^-\gamma$	0.167	'pipi'

Table 2: Possible background processes with the corresponding cross section

For e^+e^- annihilation data, the magnitude of the thrust vector varies between 0.5 (for spherical events) and 1 (for events with all tracks aligned with the thrust axis). The distribution of the thrust value (see left plot of Figure5) of τ-pair production indicates that the τ lepton decay particles deviate relatively mild from the primary trajectory.

The total CMS visible energy of the event can be used to reduce the background contaminations further through a threshold cut (see right plot of Figure5). The visible energy distribution clearly shows that there are undetected neutrinos in the signal events which shift the distribution towards smaller values. This is in contrast to some of the background processes, such as $ee\gamma$, where the visible energy peaks near the collision energy $\sqrt{s}$.

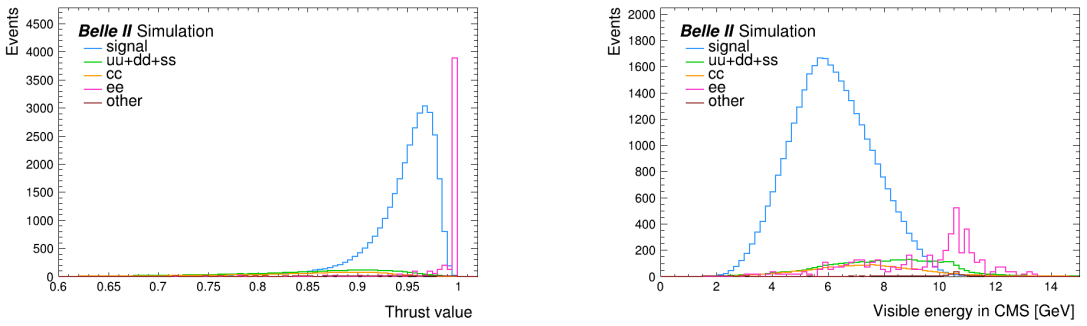

Figure 5: The MC distribution of the thrust value (left) and visible energy in CMS (right). All the samples are scaled to the luminosity of the proc9 data

The obvious difference in shapes of the kinematic distributions allows to suppress the background contaminations. The figure of merit (FOM),

$$FOM = \frac{S}{\sqrt{S+B}}, \tag{2}$$

is used for the cut value optimisation. Here, S is number of signal events, while B is number of total background events normalised according to their relative branching fractions. The distributions of the FOM for the thrust value and visible energy are shown on Figure6 . The actual requirements are indicated as dash lines.

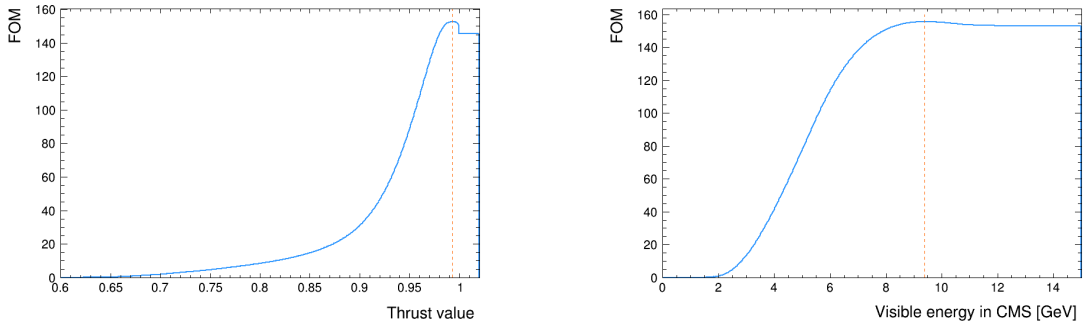

Figure 6: The FOM distributions for thrust value (left) and visible energy in CMS (right). The dash lines indicate the maximum of FOM

Finally, selections are applied to the number of photons in the event to account for initial and final state radiation, as well as the potential presence of π^0 . All events are required to have at most one π^0 and at most one additional photon on the tag-side. No photons and no π^0s are required on the signal side. The complete list of background suppression cuts are summarized in Table3.

variable	requirement imposed
thrust value	< 0.99
visible energy in CMS	$< 9.38\ GeV$
N_{γ}^{sig}	$= 0$
$N_{\pi_0}^{sig}$	$= 0$
N_{γ}^{tag}	< 2
$N_{\pi_0}^{tag}$	< 2

Table 3: Summary of the background suppression cuts.

Figure7 shows the distributions of thrust and visible energy after all the above mentioned cuts are applied. It's nice to see almost all backgrounds have been suppressed.

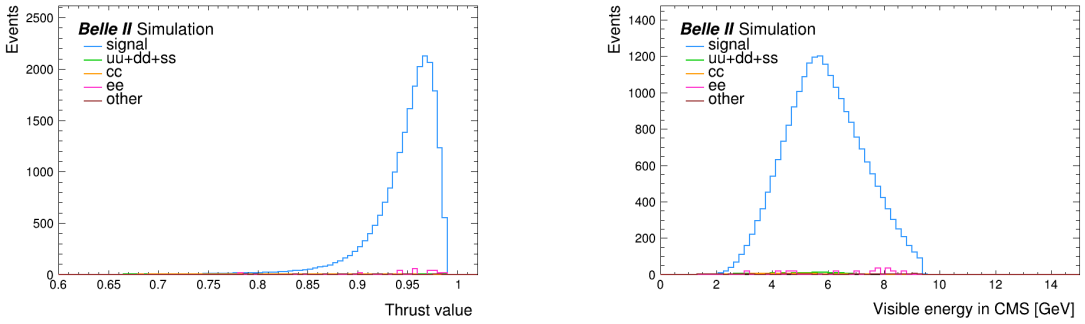

Figure 7: The MC distribution of the thrust value and visible energy in CMS after the background suppresion requirements. All the samples are scaled to the luminosity of the proc9 data

4.3 Trigger

Considering the efficiency of trigger firing is not 100%, then it is important to take trigger efficiency into account before comparing data and MC.

The energy-based ECL trigger (bit 27) is fired for events in data, which has been shown to have higher efficiency than the track-based CDC trigger (bit 0) for events entering this analysis. This trigger requires the ECL energy to be above 1 Gev, and vetos events if they are also fire the Bhabha trigger.

After the above mentioned trigger requirement for data, it's important to account for the trigger efficiency in MC. Although the trigger information is not available in the MC12 samples, we can calculate the efficiency from data and reweight the MC accordingly.

We use an CDC trigger as a reference trigger for probing the ECL trigger efficiency. The particular reference trigger considered is bit 0. It requires at least three two-dimensional tracks. We define the trigger efficiency as:

$$\epsilon_{ECL}^{trig} = \frac{fire\ trigger\ bit\ 27\ and\ bit\ 0}{fire\ trigger\ bit\ 0}, \tag{3}$$

The measured ECL trigger efficiency in data for thrust and visible energy are shown in Figure8.

5 Results

5.1 Data-MC comparison

After applying all of the previously mentioned selections, it is important to check how well our MC models the observed data. The distributions of the thrust and visible energy after the pre-selections are shown in Figure9, and the same distributions after the background suppresion requirements are shown in Figure10.

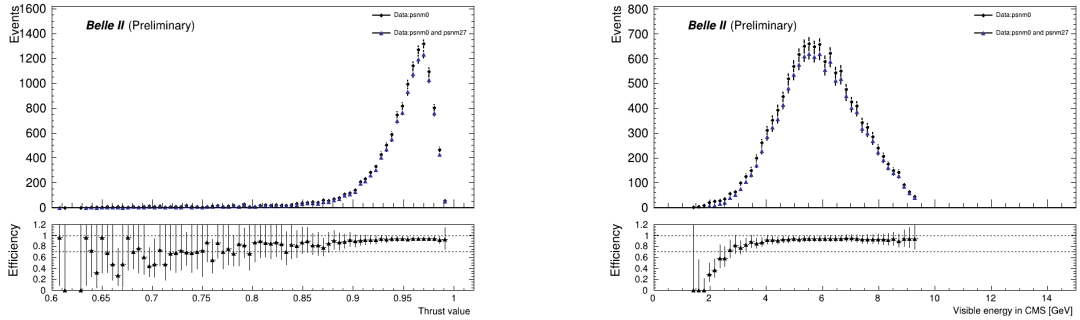

Figure 8: The number of events in data that fire the reference CDC trigger (bit 0) and, in addition, the ECL trigger (bit 27). The ratio,which corresponds to the ECL trigger efficiency, is shown in the bottom panel.

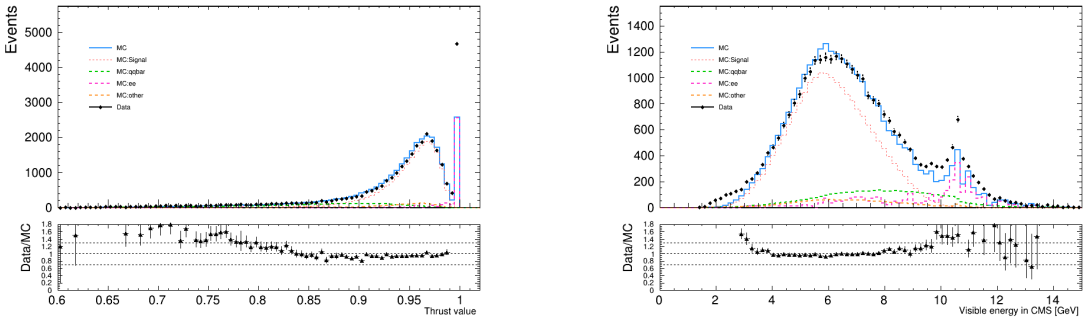

Figure 9: Comparison of data and MC of the thrust and visible energy distributions after the pre-selections. The bottom panel shows the ratio of the data and total MC prediction.

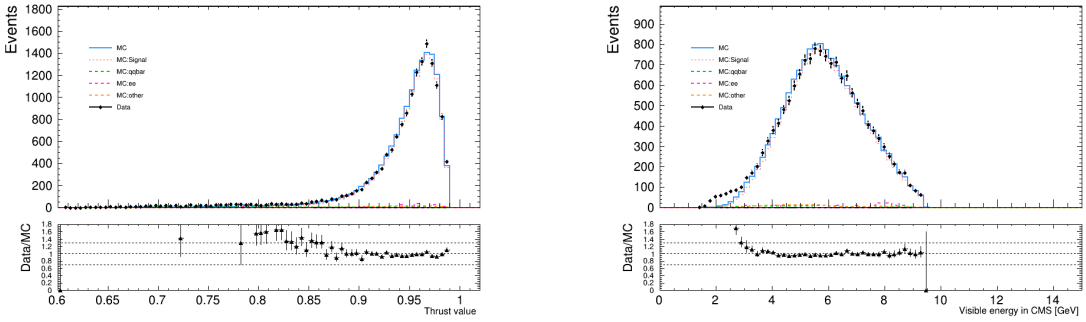

Figure 10: Comparison of data and MC of the thrust and visible energy distributions after the background suppresion requirements. The bottom panel shows the ratio of the data and total MC prediction.

It is important to note that in Figure10 there is still no trigger requirement, and it's obvious to see there still exits discrepancy between data and MC.

After reweighting MC by the measured trigger efficiency in data, the resulting thrust, visible energy distributions are shown in Figure11. As can be seen form Figure11, the discrepancy diminishes and there is a good agreement between data and MC after trigger correction. After all selections, 14072 events are observed in data with an expected purity of $14.5 \pm 0.04\%$.

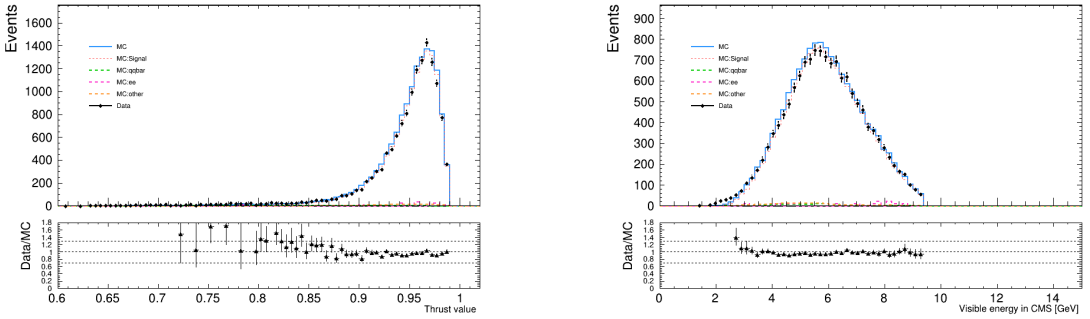

Figure 11: Comparison of data and MC of the thrust and visible energy distributions after the background suppresion and trigger requirements. MC is reweighted according to the trigger efficiency measured in data. The bottom panel shows the ratio of the data and total MC prediction.

5.2 BR measurement

The branching ratio for a decay process is the fraction of particles which decay by an individual decay mode with respect to the total number of particles which decay. The branching ratio is given by:

$$BR = \frac{N_{data}^{sig}}{\sigma \cdot L \cdot BR_{tag} \cdot \epsilon_{trig} \cdot \epsilon_{sig}}, \tag{4}$$

where N_{data}^{sig} is the number of signal events in data after all selections, σ is the cross section of $e^+e^- \to \tau^+\tau^-$, L is luminosity of experiment 8, BR_{tag} is the branching ratio of the tag side decay ($15.21 \pm 0.06\%$, from PDG), ϵ_{trig} is the ECL trigger efficiency and ϵ_{sig} is the signal efficiency.

The signal efficiency is calculated from Monte Carlo simulation:

$$\epsilon_{sig} = \frac{N_{MC}^{sig}}{BR_{tag} \cdot BR_{\tau \to e\nu\nu} \cdot N_{gen}}, \tag{5}$$

where N_{MC}^{sig} is the number of signal events in MC after all selections, BR_{tag} is the branching ratio of tag side and N_{gen} is the number of generated signal events in MC.

variable	value	Comments
N_{MC}^{sig}	577226	
N_{gen}	73.52×10^6	
BR_{tag}	$(15.21 \pm 0.06)\%$	source: PDG
$BR(\tau \to e\nu\nu)$	$(17.82 \pm 0.04)\%$	source: PDG
N_{data}^{sig}	14072	
σ	0.919 nb	
ϵ_{trig}	$(96.1 \pm 0.17)\%$	

Table 4: Summar of values for branching ratio measurement

Substituting the values from Table4 into eqution(5) and eqution(4), the branching ratio value is measured to be:

$$BR(\tau \to e\nu\nu) = (17.46 \pm 0.16)\% \tag{6}$$

6 Conclusion

The aim of this project was to analyise Belle II data in order to reconstruct $e^+e^- \to \tau^+\tau^-$ events, and finally measure the branching ratio for $\tau \to e\bar{\nu}\nu$. Using $1.9fb^{-1}$ of early Belle II data, the $\tau \to e\bar{\nu}\nu$ branching ratio was measured to be $(17.46 \pm 0.16)\%$. Only statistical uncertainies are considered. This is in reasonable agreement with the PDG value of $(17.82 \pm 0.04)\%$.

7 Appendix

7.1 Additional plots for the distribution of mass

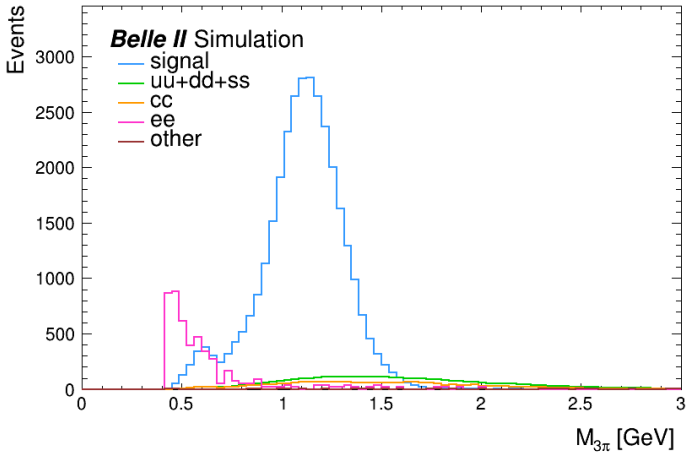

Figure 12: The MC distribution of the mass of 3-prong after pre-selections. All the samples are scaled to the luminosity of the proc9 data

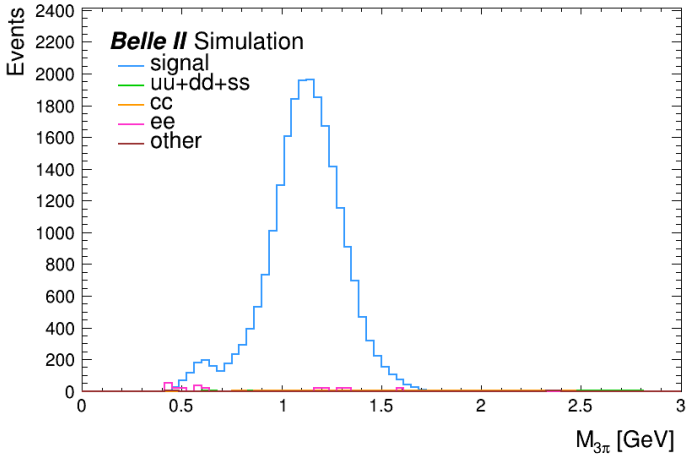

Figure 13: The MC distribution of the mass of 3-prong after the background suppresion requirements. All the samples are scaled to the luminosity of the proc9 data

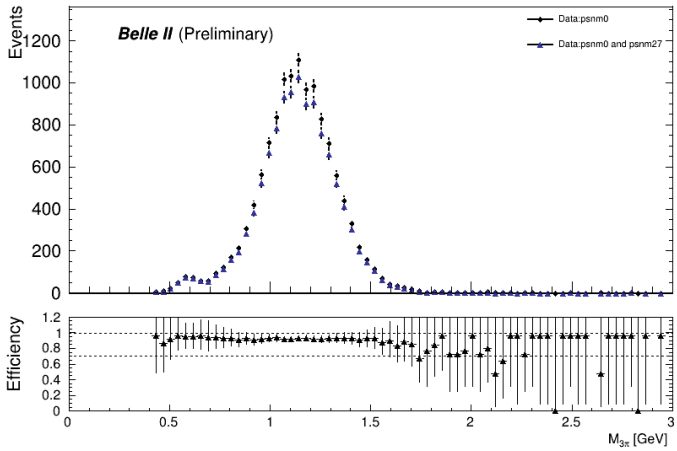

Figure 14: The number of events in data that fire the CDC trigger (bit 0) and, in addition, the ECL trigger (bit 27). The ratio,which corresponds to the ECL trigger efficiency, is shown in the bottom panel.

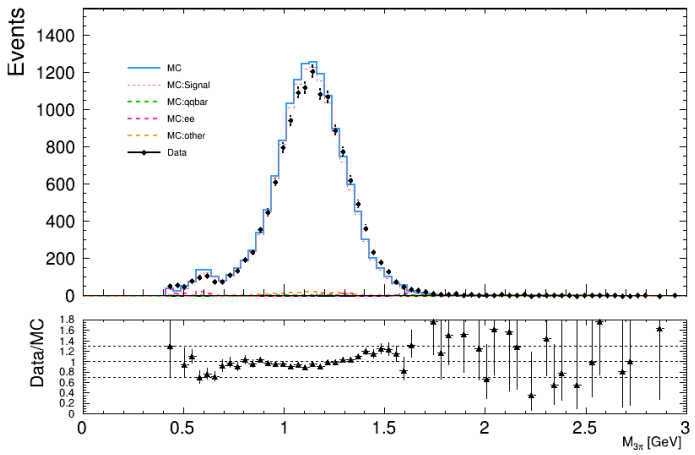

Figure 15: Comparison of data and MC of the mass of 3-prong after the background suppresion and trigger requirements. MC is reweighted according to the trigger efficiency measured in data. The bottom panel shows the ratio of the data and total MC prediction.

7.2 Additional CDC trigger efficiency plots

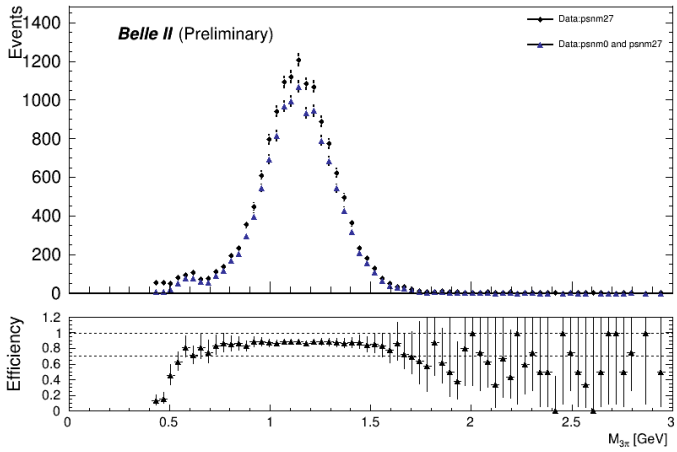

Figure 16: The number of events in data that fire the CDC trigger (bit 0) and, in addition, the ECL trigger (bit 27). The ratio,which corresponds to the CDC trigger efficiency, is shown in the bottom panel.

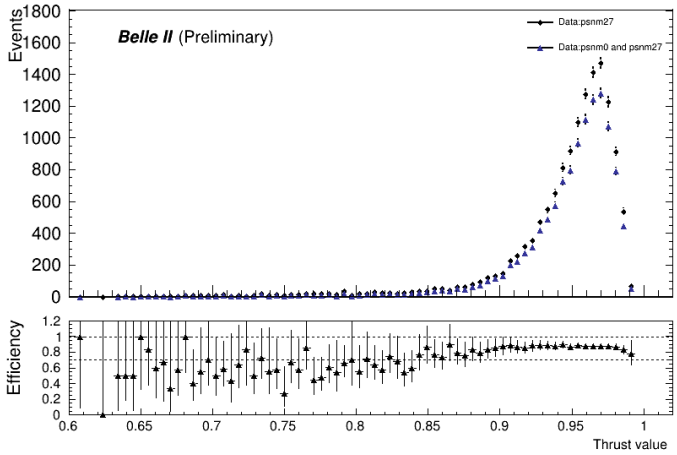

Figure 17: The number of events in data that fire the CDC trigger (bit 0) and, in addition, the ECL trigger (bit 27). The ratio,which corresponds to the CDC trigger efficiency, is shown in the bottom panel.

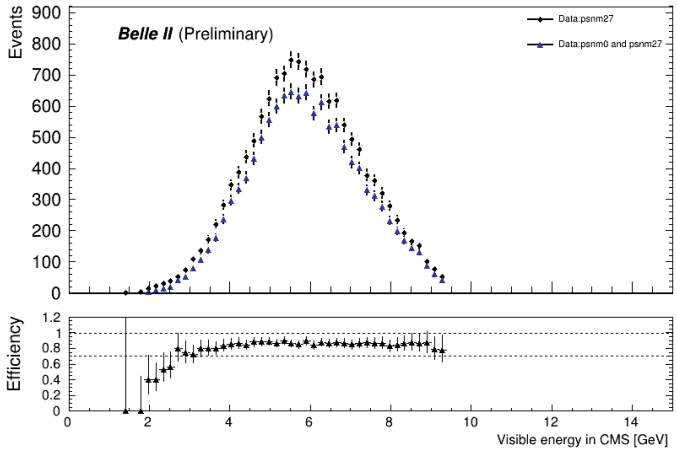

Figure 18: The number of events in data that fire the CDC trigger (bit 0) and, in addition, the ECL trigger (bit 27). The ratio,which corresponds to the CDC trigger efficiency, is shown in the bottom panel.

7.3 Additional plots for Data/MC pull

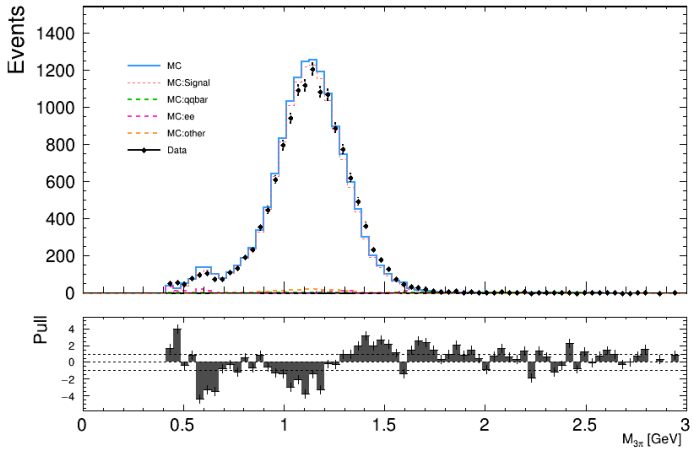

Figure 19: Comparison of data and MC of the mass of 3-prong after the background suppresion and trigger requirements. Events in data are required to fire ECL trigger. MC is reweighted according to the trigger efficiency measured in data. The bottom panel shows the pull of the data and total MC prediction.

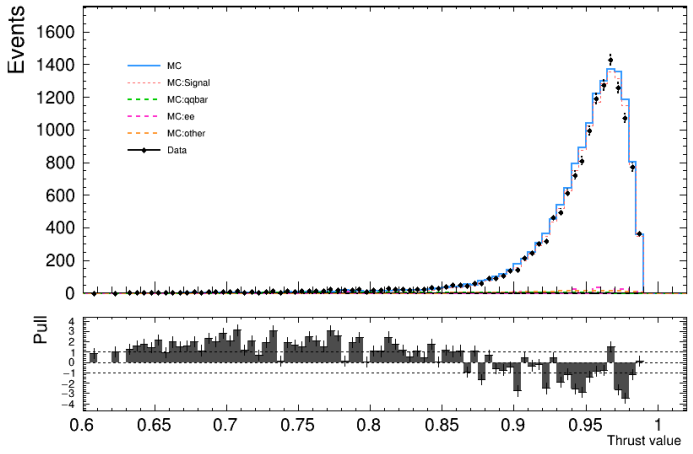

Figure 20: Comparison of data and MC of the after the background suppresion and trigger requirements. Events in data are required to fire ECL trigger. MC is reweighted according to the trigger efficiency measured in data. The bottom panel shows the pull of the data and total MC prediction.

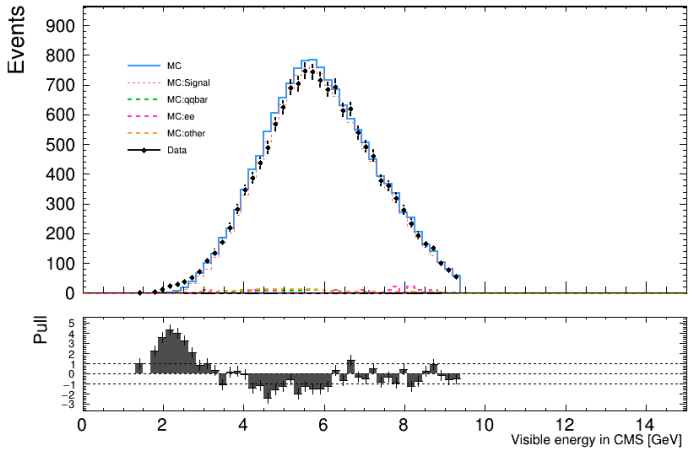

Figure 21: Comparison of data and MC of the visible energy after the background suppresion and trigger requirements . Events in data are required to fire ECL trigger. MC is reweighted according to the trigger efficiency measured in data. The bottom panel shows the pull of the data and total MC prediction.

7.4 Additional photon and π^0 multiplicity plots for Data/MC

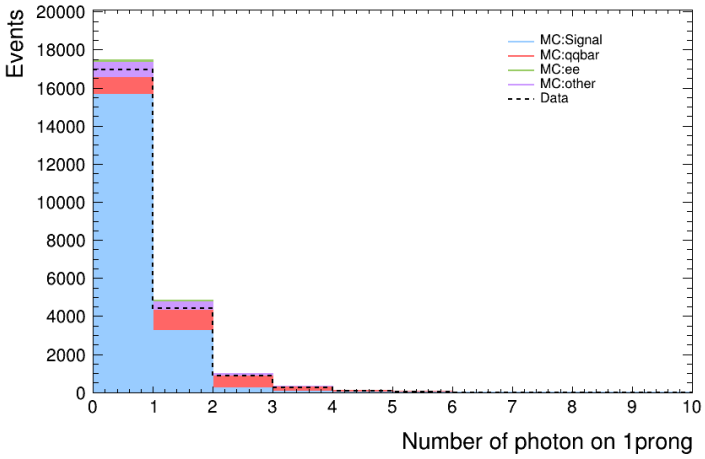

Figure 22: Photon multiplicity on 1-prong side.

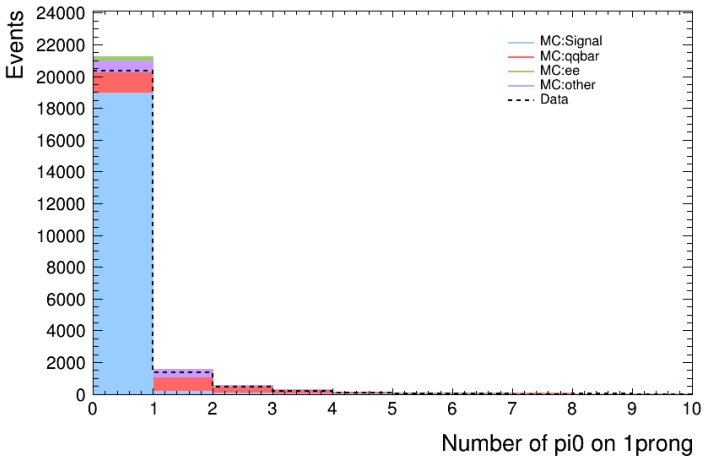

Figure 23: π^0 multiplicity on 1-prong side.

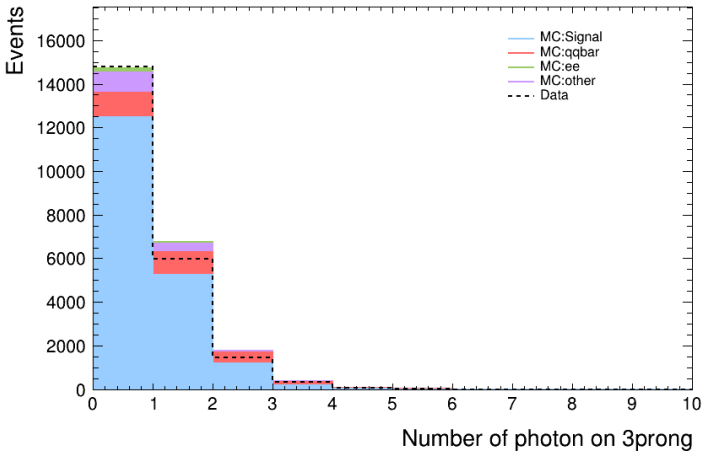

Figure 24: Photon multiplicity on 3-prong side.

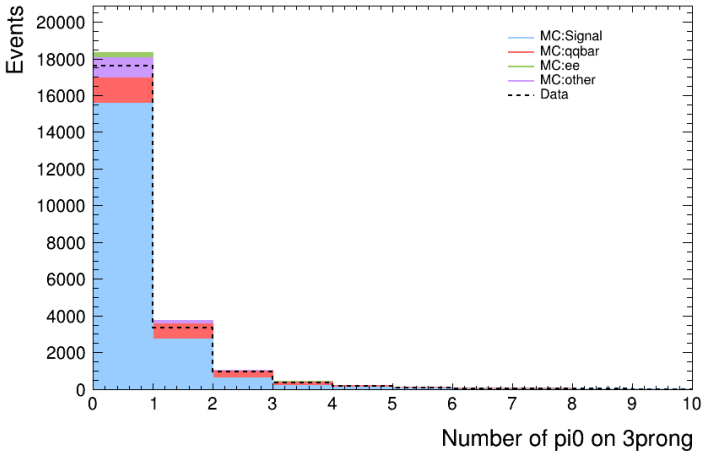

Figure 25: π^0 multiplicity on 3-prong side.

References

[1] $e^+e^- \to \tau^+\tau^-$ production and the τ lepton mass measurement at Belle II, *P. Rados, A. Rostomyan, and F. Tenchini.*

[2] τ-lepton Studies within Belle II Experiment, *Yurii Kvasiuk, Taras Shevchenko National University of Kyiv, Ukraine*

[3] Prospects for τ lepton physics at Belle II, *M. Hernndez Villanuevaet al.*